

# FusionRegister: Every Infrared and Visible Image Fusion Deserves Registration

Congcong Bian<sup>1</sup> Haolong Ma<sup>1</sup> Hui Li<sup>1\*</sup> Zhongwei Shen<sup>2</sup>  
Xiaoqing Luo<sup>1</sup> Xiaoning Song<sup>1</sup> Xiao-jun Wu<sup>1</sup>

<sup>1</sup> School of Artificial Intelligence and Computer Science, Jiangnan University, Wuxi, China

<sup>2</sup> School of Electronic and Information Engineering, Suzhou University of Science and Technology, Suzhou, China

bociic-jnu-cv@163.com, ninesxd@qq.com, {lihui.cv, xluo, x.song, wu-xiaojun}@jiangnan.edu.cn  
shenzw@usts.edu.cn

## Abstract

Spatial registration across different visual modalities is a critical but formidable step in multi-modality image fusion for real-world perception. Although several methods are proposed to address this issue, the existing registration-based fusion methods typically require extensive pre-registration operations, limiting their efficiency. To overcome these limitations, a general cross-modality registration method guided by visual priors is proposed for infrared and visible image fusion task, termed FusionRegister. Firstly, FusionRegister achieves robustness by learning cross-modality misregistration representations rather than forcing alignment of all differences, ensuring stable outputs even under challenging input conditions. Moreover, FusionRegister demonstrates strong generality by operating directly on fused results, where misregistration is explicitly represented and effectively handled, enabling seamless integration with diverse fusion methods while preserving their intrinsic properties. In addition, its efficiency is further enhanced by serving the backbone fusion method as a natural visual prior provider, which guides the registration process to focus only on mismatch regions, thereby avoiding redundant operations. Extensive experiments on three datasets demonstrate that FusionRegister not only inherits the fusion quality of state-of-the-art methods, but also delivers superior detail alignment and robustness, making it highly suitable for infrared and visible image fusion method. The code will be available at <https://github.com/bociic/FusionRegister>.

## 1. Introduction

In recent years, Infrared and Visible Image Fusion (IVIF) has made significant progress. Non-deep learning methods achieve efficient information selection and adaptive fu-

\*Corresponding author

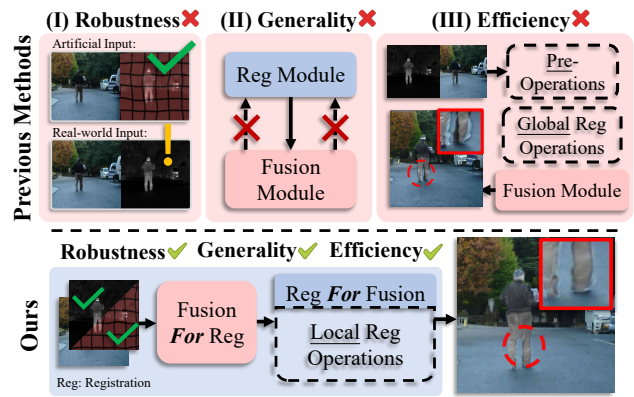


Figure 1. Existing registration-based fusion methods face three key limitations: (I) Depend on artificial deformations; (II) Cannot interact with fusion methods; (III) Require extensive pre-operations and global registration. We propose a visual prior-based post-registration method that leverages fusion results to preserve fusion quality while significantly enhancing structural accuracy, achieving efficiency and robustness.

sion [9, 17, 28, 33]. Deep learning-based approaches further exploit the power of neural models to extract both shared and modality-unique features for more accurate fusion [18, 21, 23, 36]. Modality-shared information refers to features that are clearly present in both modalities, while modality-unique information represents those observable only in one modality [25]. However, due to limitations of imaging devices, infrared and visible images are often misaligned. Direct fusion of unregistered images leads to severe information displacement, degrading fusion quality and overall efficiency.

To address the above drawback, many studies have focused on registration as a pre-processing step. Existing methods, including image- or feature-level registration, utilize style transfer to reduce modality discrepancies, simplifying optical flow prediction [47, 48]. However, style transfer often incurs high computational cost and inevitable

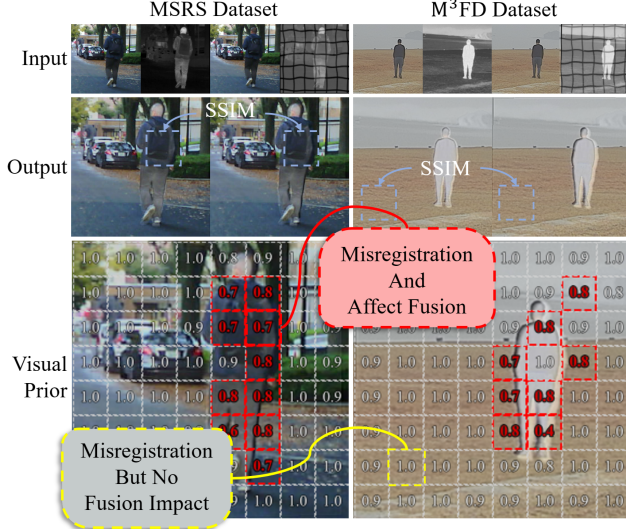


Figure 2. The fusion results show that even with spatial deformation in the infrared image, misregistration appears only in modality-shared regions, where structural similarity with the fine registered result is significantly reduced.

information loss. Other approaches map modality-specific features into a latent shared space to extract aligned representations [51, 52]. More recent works predict offset parameters directly in the intermediate feature domain, enabling one-stage fusion of aligned features [22, 24]. Nevertheless, as shown in Fig. 1, most existing cross-modal registration strategies still depend on computationally intensive pre-alignment operations to disentangle and align modal information, which limits their generality and computational efficiency.

Moreover, most registration-based fusion methods attempt to align all information from both modalities during fusion, ignoring a key fact of image fusion: **NOT ALL features are preserved in the fused image**. As shown in Fig. 2, we take two perfectly registered pairs of a visible image  $I_{vi}$  and an infrared image  $I_{ir}$ , and apply a spatial transform to create two misaligned pairs  $I_{vi}$  and  $I_{ir}^\phi$ . All pairs are processed by the same image fusion backbone [7] to generate fused results  $I_f$  and  $I_f^\phi$ . Patch-level similarity analysis shows that spatial misregistration in the infrared image mainly affects the modality-shared regions, while the modality-specific regions remain mostly unchanged. This suggests that post-registration is only needed in the misaligned regions, ensuring accurate fusion without redundant global registration or heavy pre-processing. Based on this visual prior, we design FusionRegister, a universal post-registration framework as shown in Fig. 1, which balances robustness, generality, and efficiency.

Furthermore, multi-modal sensors are typically positioned in close proximity, naturally providing coarse registration between modalities. This implies that registration-joint fusion methods should be capable of directly han-

dling raw sensor inputs. Nevertheless, many state-of-the-art methods rely on artificially generated deformations as supervisory signals, forcing networks to learn registration parameters from synthetic perturbations. As a result, these methods tend to collapse when confronted with real-world inputs that lack such deformations.

In contrast, our method focuses on learning and localizing misregistration representations, thereby enabling targeted correction within affected regions. This design enhances the robustness of fusion methods, allowing the fusion network to perform reliably on both deformed and clean inputs.

Moreover, evaluating registration quality in IVIF also remains challenging due to the lack of perfectly aligned reference pairs. Existing metrics rely on synthetic distortions, which fail to reflect real-world misregistration. To enable fair and structure-aware evaluation, we employ the Segment Anything Model (SAM) [16] to obtain unbiased structural masks. This combination provides a consistent and fine-grained measure of registration accuracy. The main contributions of this work are summarized as follows:

- A novel post-registration paradigm using visual priors that preserves fusion quality while significantly improving registration accuracy is proposed, demonstrating strong generality across diverse fusion methods.
- A general framework seamlessly integrated with various infrared-visible fusion approaches is introduced, efficiently addressing cross-modal misregistration with minimal computational overhead.
- A robust misrepresentation learning mechanism tailored to real-world scenarios is designed, capturing diverse misregistration representation to enhance adaptability across challenging conditions.

## 2. Related Work

### 2.1. Infrared and Visible Image Fusion

Early deep learning-based IVIF methods mainly rely on CNNs for feature extraction and fusion. Liu et al. [34] apply CNNs to this task, revealing the potential of end-to-end learning but suffering from limited representation and high complexity. To improve efficiency, [7, 23] introduces low-rank representation and distillation. AE-based frameworks [18–21] are then proposed to enhance multi-scale and structural representation and progressively improve feature interaction and reconstruction quality.

To reduce dependence on paired data and improve perceptual realism, GAN-based methods introduce unsupervised adversarial learning. FusionGAN [36] pioneers this direction, and DDcGAN [37] enhances detail sharpness through dual discriminators, inspiring attention- [27], frequency- [49], and gradient-based [39] variants. Transformer-based models [3, 4, 12, 32, 46, 54] further

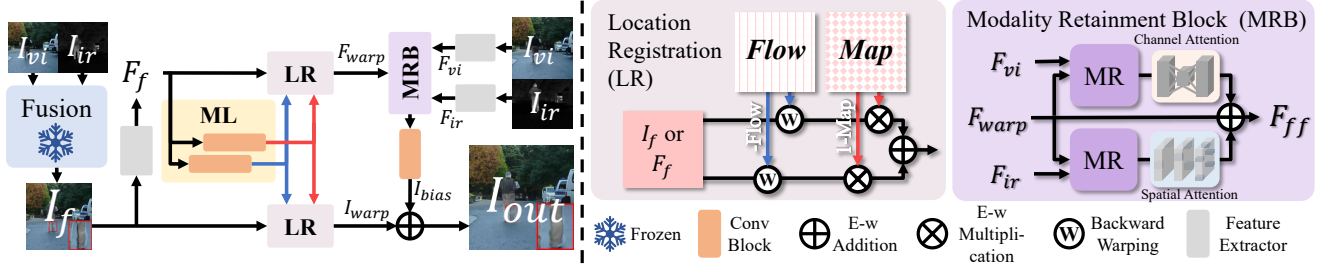


Figure 3. The proposed FusionRegister consists of two core components: post-registration of misregistration regions via bi-directional warping, and a modality retainment block (MRB). Note that ML is misregistration location operation and e-w denotes element-wise.

advance IVIF by modeling long-range dependencies and global semantics and extend fusion via textual and prompt guidance to resolve semantic ambiguity.

Recently, diffusion and state-space models push IVIF toward higher fidelity and scalability. [11, 38, 43, 44, 53, 55] improve consistency through diffusion generation. S4Fusion [35] and MambaDFuse [29] further achieve lightweight long-range modeling with state-space dynamics.

Based on the above discussions, in this work, five representative methods from these paradigms are used to evaluate the generalization of FusionRegister.

## 2.2. Registration-joint IVIF

In real world scenarios, the misalignment between multi-modal sensors remains a major challenge in IVIF, as imperfect alignment causes ghosting and distortion. Style transfer mitigate modality gaps [1, 48]. [13, 51, 52] try coarse-to-fine registration combining rigid and non-rigid stages.

To avoid information bias caused by pre-operations, feature-level strategies such as IVFWSR [22] and RFVIF [24] directly align latent representations to improve fusion under misalignment, while MulFS-CAP [26] and SemLA [50] leverage modality dictionaries and semantic priors for more robust matching.

However, most existing registration-fusion frameworks still follow a “register-then-fuse” paradigm, incurring high preprocessing cost and weak adaptability. In contrast, our approach performs fusion first and then corrects misaligned regions guided by visual priors, ensuring both robustness and efficiency with new fusion models.

## 3. Methodology

### 3.1. Overview

The proposed method, FusionRegister, aims to correct spatial misregistration that persists after image fusion while preserving modality-specific details.

Given a visible image ( $I_{vi}$ ), an infrared image ( $I_{ir}$ ), and their fused result ( $I_f$ ), FusionRegister refines the fusion by

localizing and correcting regions affected by misregistration, guided by visual priors embedded between  $I_f$  and  $I_{gt}$ .  $I_{gt}$  is the perfectly registered fused image.

As illustrated in Fig. 3, FusionRegister follows a visual prior guided pipeline composed of three collaborative stages: (1) *Misregistration Localization (ML)*, which detects spatial inconsistencies and estimates deformation fields; (2) *Location Registration (LR)*, which performs bi-directional warping to realign misregistered regions without damaging well-aligned ones; (3) *Modality Retainment Block (MRB)*, which compensates texture and structure losses introduced during spatial transformation.

### 3.2. Misregistration Localization and Location Registration

FusionRegister processes inputs in a hierarchical manner inspired by MIMO-UNet [5]. At each scale  $i \in \{0, \dots, N-1\}$ , downsampled versions  $I_{in}^i$  ( $in \in \{f, vi, ir\}$ ) are extracted, and three feature extractors that have the same structure but different parameters produce multi-scale features:

$$F_{in}^0, \dots, F_{in}^{N-1} = FE_{in}(I_{in}^0, \dots, I_{in}^{N-1}), \quad (1)$$

$$in \in \{f, vi, ir\},$$

where  $I_{in}^0$  is source image, and  $I_{in}^i \in \mathbb{R}^{B \times 3 \times (H/2^i) \times (W/2^i)}$ . Detailed extractor architecture is provided in the supplementary material.

**Misregistration Localization (ML)** estimates a probability map  $M^i \in \mathbb{R}^{B \times 1 \times (H/2^i) \times (W/2^i)}$  and a deformation field  $\phi^i \in \mathbb{R}^{B \times 2 \times (H/2^i) \times (W/2^i)}$  that jointly represent the location and magnitude of misregistration. The field  $\phi^i$  is progressively refined from coarse to fine levels:

$$\phi^i = \phi^i \otimes (1 \oplus 2 \otimes Up(\phi^{i+1})), \quad (2)$$

where  $\oplus$  and  $\otimes$  denote element-wise addition and multiplication, respectively.  $Up(\cdot)$  indicates bilinear upsampling. The factor of “2” in Eq. 2 serves as a scaling coefficient applied to the upsampled deformation field  $\phi^{i+1}$  to compensate for the resolution mismatch and maintain the physical

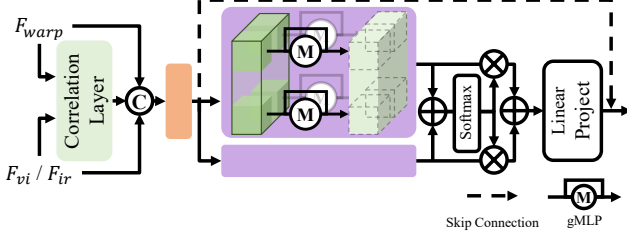


Figure 4. Detailed architecture of the Modality Retainment Block (MRB).

consistency. This hierarchical propagation ensures spatial coherence and suppresses isolated deformations.

Compared with existing deformation field-based registration-based fusion frameworks, FR abandons the reliance on globally supervised guidance. Instead, it leverages visual prior cues to adaptively capture spatial misregistration representation and infer localized deformation transformations, enabling a more robust and generalizable field-free supervised paradigm.

**Location Registration (LR)** applies the predicted  $\phi^i$  to correct the fused feature and fused image. Traditional single-direction backward warping may cause tearing or over-compensation. Thus, FusionRegister adopts a bi-directional warping strategy that symmetrically compensates distortions:

$$I_{\text{warp}}^i = M^i \otimes BW(I_f^i, \phi^i) \oplus (1 - M^i) \otimes BW(I_f^i, -\phi^i), \quad (3)$$

$$F_{\text{warp}}^i = M^i \otimes BW(F_f^i, \phi^i) \oplus (1 - M^i) \otimes BW(F_f^i, -\phi^i), \quad (4)$$

where  $BW(\cdot)$  denotes backward warping. The combination of forward and reverse corrections stabilizes deformation and prevents edge tearing. The resulting  $F_{\text{warp}}^i$  is passed to MRB for detail restoration.

### 3.3. Modality Retainment Block

Spatial warping often weakens texture and attenuates contrast. To recover fine-grained information, we introduce the Modality Retainment Block (MRB). As shown in Fig. 4, a lightweight module leveraging gated MLP(gMLP) [30] to enhance cross-modal feature retention.

Firstly, a Correlation Layer [15] (Fig. 5) measures local correspondence between the warped fusion feature  $F_{\text{warp}}^i$  and source features  $F_{\text{src}}^i$  ( $\text{src} \in \{vi, ir\}$ ). By zero-padding  $F_{\text{src}}^i$  with a range of  $p$ , resulting in a padded source feature  $\tilde{F}_{\text{src}}^i \in \mathbb{R}^{B \times 2^i C \times (H/2^i + 2p) \times (W/2^i + 2p)}$ . Then,  $\tilde{F}_{\text{src}}^{i,m,n} \in \mathbb{R}^{B \times 2^i C \times (H/2^i) \times (W/2^i)}$  is the source feature map  $F_{\text{src}}^i$  spatially shifted by  $m$  pixels horizontally and  $n$  pixels vertically in  $\tilde{F}_{\text{src}}^i$ ,  $m, n \in \{0, \dots, 2p\}$ .  $\tilde{F}_{\text{src}}^{i,m,n}$  are compared with  $F_{\text{warp}}^i$  to generate a correlation descriptor:

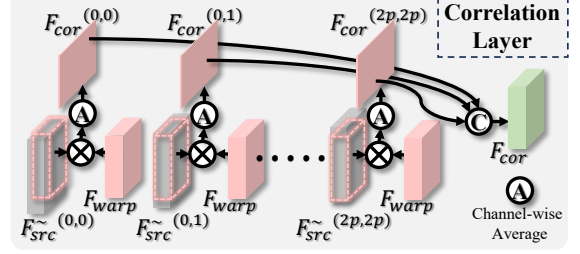


Figure 5. Detailed architecture of the Correlation Layer.

$$F_{\text{cor}}^{i,m,n} = CA(\tilde{F}_{\text{src}}^{i,m,n} \otimes F_{\text{warp}}^i), \quad (5)$$

where  $CA(\cdot)$  denotes channel-wise averaging. All  $F_{\text{cor}}^{i,m,n}$  are concatenated to form the final correlation feature  $F_{\text{cor}}^i \in \mathbb{R}^{B \times 4p^2 \times (H/2^i) \times (W/2^i)}$ .  $F_{\text{cor}}^i$  serves as a bridge, recording local geometric relationships under multiple offsets. The concatenated features of  $F_{\text{warp}}^i$ ,  $F_{\text{src}}^i$ , and  $F_{\text{cor}}^i$  are compressed through a convolution block.

The compressed feature is partitioned into non-overlapping patches with different scales  $s$ . The gMLP models spatial interactions through channel mixing and gating, enabling efficient long-range dependency modeling without self-attention. For an input patch  $F_{\text{cor}}^{i(s)} \in \mathbb{R}^{B \times 2^i C \times s \times s}$ , gMLP applies a channel projection and a spatial gating unit:

$$F_{\text{cor}}^{i(s)} = (F_{\text{cor}}^{i(s)} W_1) \otimes \sigma((F_{\text{cor}}^{i(s)} W_2) \mathbf{G}), \quad (6)$$

where  $W_1, W_2$  are linear projections,  $\mathbf{G}$  is a learned gating matrix,  $\sigma(\cdot)$  is ReLU function. All patches  $F_{\text{cor}}^{i(s)}$  are concatenated back in their original spatial order to reconstruct the  $F_{gMLP}^{i(s)}$ . A softmax-weighted aggregation produces the final retained feature  $F_{gMLP}^i$ :

$$F_{gMLP}^i = \sum_s w_s \cdot F_{gMLP}^{i(s)}, \quad (7)$$

where  $w_s$  indicates the softmax weight of each scale  $s$ .

To emphasize modality-specific information, MRB integrates dual attention mechanisms:

- *Visible-modality attention* enhances semantic consistency through channel weighting:

$$F_{f\&vi}^i = F_{gMLP}^i \otimes (\text{Sig}(\text{Conv}(\text{SA}(F_{gMLP}^i)))) \oplus 1, \quad (8)$$

where  $\text{SA}(\cdot)$  denotes spatial average pooling and  $\text{Sig}(\cdot)$  is the Sigmoid function.

- *Infrared-modality attention* emphasizes high-frequency details using spatial fusion:

$$F_{f\&ir}^i = F_{gMLP}^i \otimes (\text{Sig}(\text{Conv}(\text{AM}(F_{gMLP}^i)))) \oplus 1, \quad (9)$$

where  $AM(\cdot)$  concatenates channel-wise max and mean responses.

The outputs are combined to form the refined feature:

$$F_{ff}^i = F_{gMLP}^i \oplus F_{f\&vi}^i \oplus F_{f\&ir}^i. \quad (10)$$

Finally, a convolution block predicts a residual bias map  $I_{bias}^i \in \mathbb{R}^{B \times 3 \times (H/2^i) \times (W/2^i)}$ , which refines the  $I_{warp}^i$ :

$$I_{out}^i = I_{warp}^i \oplus I_{bias}^i. \quad (11)$$

### 3.4. Loss Function

The total loss jointly minimizes registration error while preserving structural and textural fidelity from both spatial and frequency domains,  $\lambda_i$  balance the four components:

$$\mathcal{L}_{all} = \lambda_1 \mathcal{L}_e + \lambda_2 \mathcal{L}_g + \lambda_3 \mathcal{L}_f + \lambda_4 \mathcal{L}_d. \quad (12)$$

Edge Loss ( $\mathcal{L}_e$ ) aligns structural boundaries of the warped and fused results ( $I_{warp}^i, I_{out}^i$ ) with the ground truth ( $I_{gt}^i$ ), via a Difference of Gaussians (DoG) extractor  $E(\cdot)$ :

$$\mathcal{L}_e = \sum_{i=0}^{N-1} \sum_{j \in \{out, warp\}} \|(E(I_j^i) - E(I_{gt}^i))\|_2, \quad (13)$$

$$E(x) = x - G(Up(Down(G(x)))) ,$$

here  $G(\cdot)$  denotes Gaussian filtering. The 1D Gaussian kernel is defined as:  $k = [0.05, 0.25, 0.4, 0.25, 0.05]$ . The 2D kernel is obtained by outer product  $G_k = k^\top k$ .

Global Spatial Loss ( $\mathcal{L}_g$ ) constrains overall structural consistency in pixel space:

$$\mathcal{L}_g = \sum_{i=0}^{N-1} \|I_{out}^i - I_{gt}^i\|_2. \quad (14)$$

Frequency Loss ( $\mathcal{L}_f$ ) preserves high-frequency texture by minimizing Fourier-domain distance:

$$\mathcal{L}_f = \sum_{i=0}^{N-1} \|FFT(I_{out}^i) - FFT(I_{gt}^i)\|_1, \quad (15)$$

where  $FFT(\cdot)$  indicates the fast Fourier transform.

Detail Loss ( $\mathcal{L}_d$ ) enhances texture consistency within misregistration map  $M^i$ , which is predicted in 3.2, through the Sobel operator  $\nabla(\cdot)$ :

$$\mathcal{L}_d = \sum_{i=0}^{N-1} \|\nabla(I_{out}^i) \otimes M^i - \nabla(I_{gt}^i) \otimes M^i\|_1. \quad (16)$$

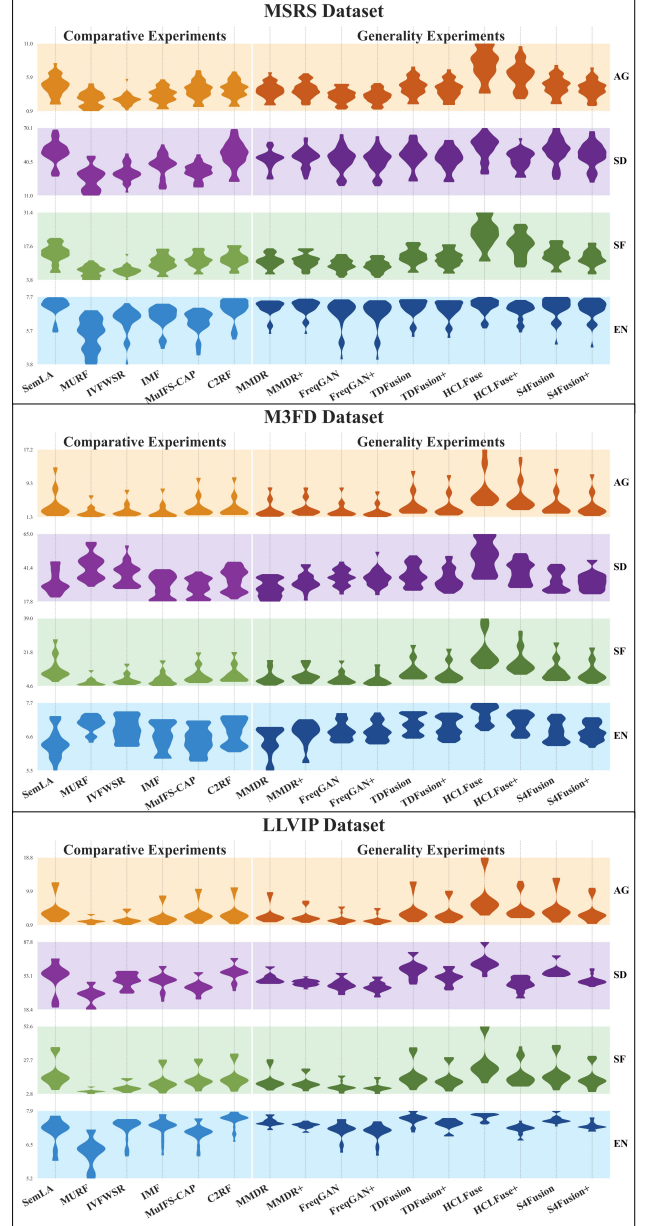


Figure 6. Image quality evaluation of FusionRegister under two scenarios. The method with “+” denotes the version aligned via FusionRegister.

## 4. Experiments

### 4.1. Implementation Details

The proposed method, FusionRegister, is trained on a new multi-modal registration dataset which is collected from the public fusion dataset (MSRS [42] and M<sup>3</sup>FD [31]). From these two fusion datasets, we manually cropped 1,333 fully registered  $260 \times 260$  patches (426 from MSRS, 907 from M<sup>3</sup>FD). For testing, 27 MSRS, 21 M<sup>3</sup>FD, and 20 LLVIP [14] samples with natural misregistration are used, evaluating at full resolution without synthetic deformation.

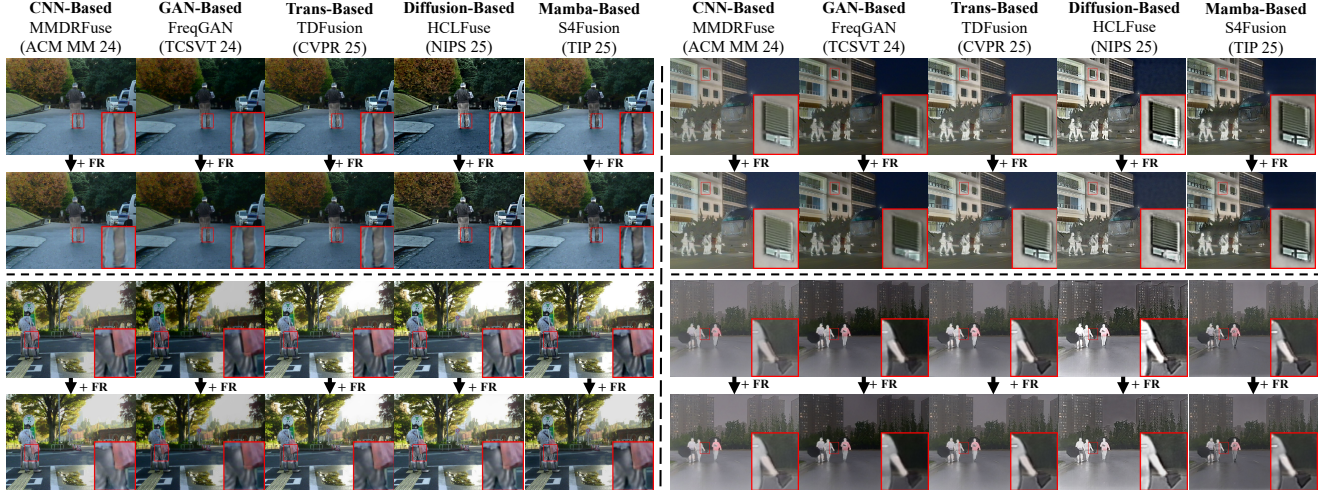


Figure 7. As a general framework, FusionRegister successfully completes post-registration for different fusion methods and scenarios, and it completely retains the high-quality fusion performance of the original methods. More qualitative experiments are provided in the supplementary material.

To simulate real-world misregistration, we apply random affine transformations to  $I_{ir}$ : rotation  $[-2^\circ, 2^\circ]$ , translation  $[-2, 2]$  pixels, scaling  $[0.95, 1.08]$ , and optional geometric operations (flips or  $90^\circ$  rotations) with 50% probability.

In the training phase, Adam ( $\beta_1 = 0.9, \beta_2 = 0.999$ ) with Cosine Annealing (lr:  $2 \times 10^{-4}$  to  $1 \times 10^{-6}$ ) is utilized. The batch size, patch size and epoch are set to 20,  $256 \times 256$ , and 5000. Hyperparameters in loss function are set as follows:  $p = 1, s \in \{1, 3\}, \lambda_1 = 10, \lambda_2 = 1, \lambda_3 = 0.1, \lambda_4 = 10$ . All experiments are implemented in PyTorch on RTX 4090 GPU.

## 4.2. Evaluation Metrics

The testing environment simulates real-world conditions, where the imaging device maintains a fixed viewpoint and only coarse cross-modal registration is available, leaving residual misalignment and no ground-truth reference  $I_{gt}$ . Evaluation is performed from two perspectives: fusion quality and registration accuracy.

For fusion quality, four no-reference metrics are adopted: EN [41] (information richness), SF [8] (texture sharpness), AG [6] (edge strength), and SD [40] (contrast). Higher values across these indicators reflect superior visual quality of the fused image.

Registration accuracy is assessed using the Segment Anything Model (SAM) [16], which performs panoramic segmentation on fused results to extract object masks. The overlap and consistency between modalities are then quantified by Intersection over Union (IoU) and PR (harmonic mean of precision and recall), where higher scores indicate better alignment. Since M<sup>3</sup>FD and LLVIP do not have segmentation labels and MSRS only has coarse annotations, manual labeling is applied to ensure fair evaluation across

datasets.

## 4.3. Generality Experiments

FusionRegister enhances registration accuracy while preserving fusion quality. To evaluate generality, we integrate FusionRegister with five representative fusion models: CNN-based (MMDRFuse [7]), GAN-based (FreqGAN [49]), Transformer-based (TDFusion [3]), Diffusion-based (HCLFuse [10]), and Mamba-based (S4Fusion [35]), all retrained under identical settings.

As shown in Fig.7, FusionRegister consistently maintains the fusion strengths of each method while correcting misregistered regions, demonstrating robustness across diverse scenarios including temporal/spatial misalignments, nighttime scenes, and motion blur. Quantitatively, FusionRegister achieves an average 5% IoU improvement for all fusion method (Table 1), confirming its potential for high-precision applications. The visualization of registration accuracy is shown in the supplementary materials.

Moreover, FusionRegister eliminates ghosting artifacts by consolidating misaligned edges into coherent structures, improving structural consistency despite minor pixel-level metric variations. Fig.6 shows post-FR results exhibit lower variance and greater stability across all frameworks. Additional visual comparisons are provided in the supplementary material.

## 4.4. Comparison Experiments

We compare six publicly available infrared-visible registration fusion methods: SemLA [50], MURF [52], IVFWSR [22], IMF [48], MulFS-CAP [26], and C<sup>2</sup>RF [45]. As shown in Fig.8, most existing approaches fail to adapt to deformation-free inputs or unseen datasets. SemLA and

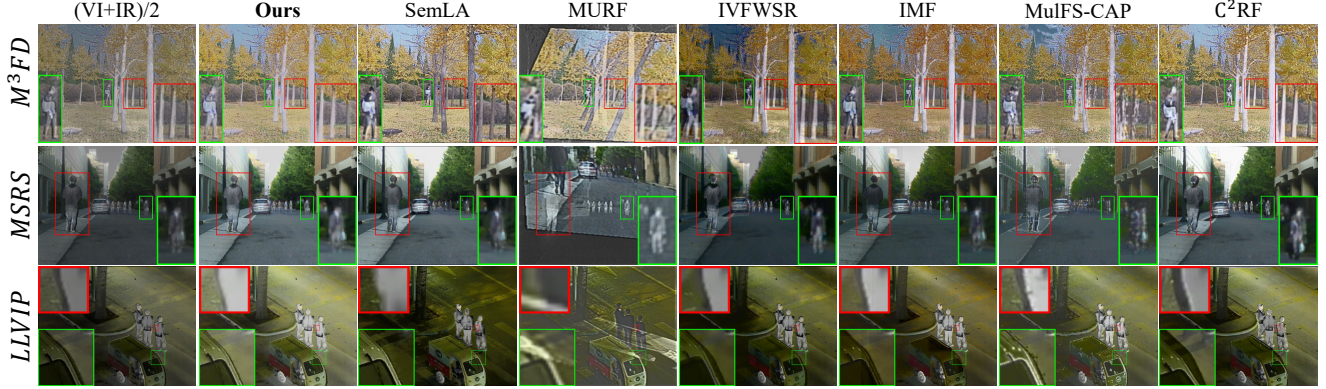


Figure 8. A comparative experiment between FusionRegister and existing registration-based fusion methods. More visual comparisons are provided in the supplementary material.

IMF, though capable of limited alignment, often collapse under low-texture or nighttime scenes, yielding blurred or unregistered results. MulFS-CAP performs well only on its training dataset (LLVIP) but generalizes poorly to MSRS and M<sup>3</sup>FD.

In contrast, FusionRegister consistently localizes and refines misregistered regions, achieving stable post-registration even on entirely unseen data. It is the only method that simultaneously preserves both object and scene integrity while ensuring precise alignment. This advantage is validated by SAM-based segmentation in Table 1 (visualized in the supplementary material) and quantitative violin-plot analyses (Fig. 6), which show that FusionRegister not only improves mean performance across six methods and three datasets but also reduces variance—demonstrating superior consistency, robustness, and adaptability. More visual comparisons are provided in the supplementary material for completeness.

## 4.5. Ablation Experiments

### 4.5.1. Effectiveness of MRB

Transformations based on deformation fields inevitably introduce geometric distortions that degrade structural consistency and fine textures. Without correction, such distortions cause local detail loss in misregistered regions. To validate the necessity of MRB, we performed an ablation study by removing it and re-evaluating fusion results. As shown in Fig. 9, the residual map  $I_{bias}$  reveals that MRB effectively restores texture details otherwise lost after deformation. The quantitative results in Table 2 further show clear declines in multiple image-quality metrics, confirming the crucial role of MRB in detail recovery, structural fidelity, and overall perceptual quality.

### 4.5.2. Effectiveness of Bi-directional warping

For comparison, we follow other deformation field-based methods that adopt one way warping with a single defor-

Table 1. Segmentation quantitative results on MSRS, M<sup>3</sup>FD and LLVIP datasets represent registration accuracy. The **bold** and **red** represent the best and second-best performance. **+FR** denote the enhanced versions with FusionRegister.

Method	MSRS		M <sup>3</sup> FD		LLVIP	
	IoU	PR	IoU	PR	IoU	PR
<i>Registration-based Fusion Methods</i>						
MURF[52]	58.3	73.3	61.3	75.1	67.3	78.4
SemLA[50]	78.7	88.4	75.0	85.9	81.0	89.7
C <sup>2</sup> RF[45]	70.5	81.5	69.4	82.6	75.4	86.1
IVFWSR[22]	64.6	79.4	70.7	83.2	75.6	86.1
IMF[48]	78.7	88.4	77.2	87.6	81.3	89.8
CAP[26]	59.1	75.6	66.7	80.6	75.5	85.9
<i>Methods with the proposed FusionRegister(FR)</i>						
MMDR[7]	83.6	91.3	76.9	87.3	83.7	90.5
<b>+FR</b>	<b>86.5↑</b>	<b>93.0↑</b>	<b>81.6↑</b>	<b>90.2↑</b>	<b>86.0↑</b>	<b>93.1↑</b>
FreqGAN[49]	80.7	89.5	74.4	85.5	82.5	90.1
<b>+FR</b>	<b>84.1↑</b>	<b>91.4↑</b>	<b>80.6↑</b>	<b>89.4↑</b>	<b>83.2↑</b>	<b>90.7↑</b>
TDFusion[2]	85.2	92.1	76.5	87.0	81.1	89.7
<b>+FR</b>	<b>86.7↑</b>	<b>92.9↑</b>	<b>81.0↑</b>	<b>89.7↑</b>	<b>82.9↑</b>	<b>90.7↑</b>
HCLFuse[10]	79.2	88.7	66.2	78.6	76.9	87.3
<b>+FR</b>	<b>83.7↑</b>	<b>91.3↑</b>	<b>80.4↑</b>	<b>89.4↑</b>	<b>84.7↑</b>	<b>91.6↑</b>
S4Fusion[35]	79.9	89.2	72.5	84.5	82.8	90.6
<b>+FR</b>	<b>85.9↑</b>	<b>92.5↑</b>	<b>75.7↑</b>	<b>86.6↑</b>	<b>85.3↑</b>	<b>92.0↑</b>

Table 2. Quantitative analysis of registration accuracy, image quality and complexity from the ablation experiments on MSRS. The **bold** and **red** represent the best and second-best

Method	Reg		Image Quality				Efficiency	
	IoU	PR	EN	SF	AG	SD	T(s)	P(M)
w/o MRB	85.6	91.9	6.92	11.46	3.95	42.71	<b>0.012</b>	<b>2.83</b>
1-d Warping	85.5	92.4	7.02	11.58	4.04	43.57	0.019	2.94
MRB w/ dt	86.0	92.3	<b>7.03</b>	11.53	3.96	<b>44.15</b>	0.025	3.21
MRB w/ dc	84.8	92.1	6.98	11.41	3.98	42.52	<b>0.014</b>	3.25
More Layers	<b>86.3</b>	<b>92.9</b>	<b>7.03</b>	<b>11.65</b>	<b>4.05</b>	43.79	0.021	7.32
Ours	<b>86.5</b>	<b>92.9</b>	7.03	<b>11.71</b>	<b>4.09</b>	<b>43.84</b>	0.019	<b>2.94</b>

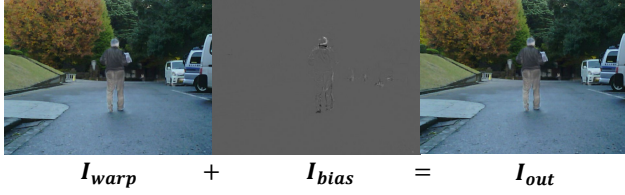


Figure 9. The MRB enables FusionRegister to preserve rich, fine-grained details.

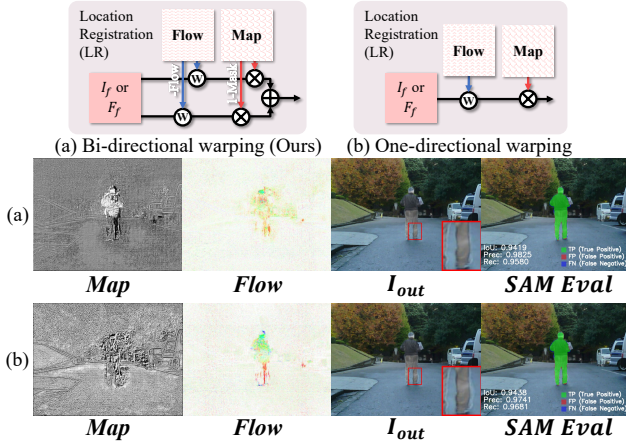


Figure 10. Bi-directional warping enables FusionRegister to achieve more precise registration.

mation field. As shown in Fig.10 (b), this one-sided strategy overemphasizes suspected misregistration regions and distorts distant structures, leading to noticeable declines in both fusion quality and registration accuracy (Table 2).

In contrast, bi-directional design leverages the mismatch map for explicit region guidance and dual fields for refined geometric correction. As illustrated in Fig.10 (a), it preserves structural integrity and recovers local textures more faithfully, confirming the advantage of the proposed mechanism.

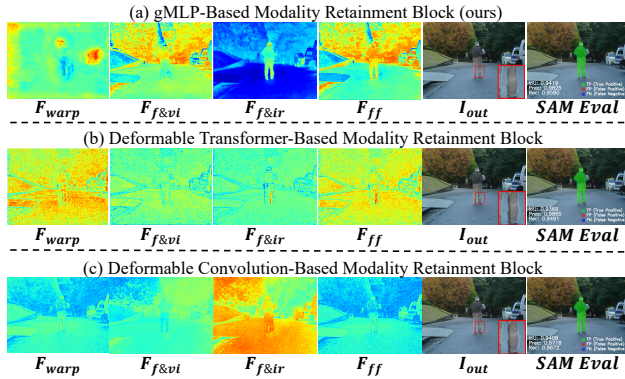


Figure 11. Implementing modality retention with gMLP leads to the extraction of more comprehensive and abundant features.

### 4.5.3. Effectiveness of Modality Retainment

The MRB employs a gMLP-based design to preserve modality-specific cues, compared against deformable convolution (DC) [56] and deformable transformer (DT) [57]. As shown in Fig.11, gMLP-MRB effectively integrates warped features ( $F_{warp}$ ) with modality cues ( $F_{f&vi}$ ,  $F_{f&tr}$ ), achieving balanced representation in  $F_{ff}$  that maintains both registration accuracy and perceptual fidelity.

In contrast, DT-MRB localizes misregistration but fails to model long-range dependencies, while the limited receptive fields yield of DC-MRB negligible improvement. Although DC offers faster inference, it lacks global modeling capacity. Table 2 confirms gMLP-MRB provides the optimal balance of alignment accuracy, detail preservation, and efficiency.

### 4.5.4. Effectiveness of Number of Network Layers

We conduct an ablation study on network depth to balance performance and efficiency. As shown in Table 2, extending from two to three layers yields marginal gains but doubles parameters and increases computation time. Considering the need for lightweight, real-time fusion, we adopt the two-layer architecture. This preserves performance while maintaining compactness, allowing computational resources to focus on misregistration correction and modality retention.

## 4.6. Complexity Comparison

We evaluate methods on two datasets. Table 3 summarizes computational costs. FR achieves the second-best efficiency. While IVFWSR is fastest, it has the largest parameters and limited adaptability. MulFS-CAP has fewest parameters but slowest inference and poor generalization. FR thus provides superior trade-offs among efficiency, generality, and quality.

Table 3. Comparison of Resource Consumption and Parameters. The **bold** and **red** represent the best and second-best performance. The **blue** represents the **WORST** performance

	SemLA	MURF	IVFWSR	IMF	CAP	C <sup>2</sup> RF	Ours
Params (M)	28.03	13.4	<b>53.8</b>	52.6	<b>1.5</b>	10.53	<b>2.94</b>
MSRS (S)	0.75	2.23	<b>0.008</b>	0.188	<b>4.5</b>	0.139	<b>0.019</b>
M <sup>3</sup> FD (S)	2.39	4.85	<b>0.013</b>	0.465	<b>10.57</b>	0.349	<b>0.057</b>

## 5. Conclusion

We present FusionRegister, a visual prior guided post-registration paradigm for infrared and visible image fusion. FusionRegister directly refines fused results by localizing and correcting misregistration regions through visual priors. This design enables focused registration, improving efficiency and robustness.

The current design of FR is limited by the assumption of coarse pre-registration. This limitation prevents FR from

achieving satisfactory performance when the inter-modal viewpoint discrepancy is significant. In future work, we will address this critical issue and explore extending the approach to a wider range of multi-modal image fusion tasks.

## 6. Acknowledgement

This work is supported by the National Key Research and Development Program of China (2023YFE0116300), the National Natural Science Foundation of China (62202205, U25A20527, 62306203), the National Key Research and Development Program of China under Grant (2023YFF1105102, 2023YFF1105105)

## References

- [1] Moab Arar, Yiftach Ginger, Dov Danon, Amit H. Bermano, and Daniel Cohen-Or. Unsupervised multi-modal image registration via geometry preserving image-to-image translation. In *IEEE/CVF Conference on Computer Vision and Pattern Recognition (CVPR)*, 2020. 3
- [2] Haowen Bai, Jianshe Zhang, Zixiang Zhao, Yichen Wu, Lilun Deng, Yukun Cui, Tao Feng, and Shuang Xu. Task-driven image fusion with learnable fusion loss. In *Proceedings of the IEEE/CVF Conference on Computer Vision and Pattern Recognition (CVPR)*, pages 7457–7468, 2025. 7
- [3] Chunyang Cheng, Tianyang Xu, Zhenhua Feng, Xiaojun Wu, Zhangyong Tang, Hui Li, Zeyang Zhang, Sara Atito, Muhammad Awais, and Josef Kittler. One model for all: Low-level task interaction is a key to task-agnostic image fusion. In *Proceedings of the Computer Vision and Pattern Recognition Conference (CVPR)*, pages 28102–28112, 2025. 2, 6
- [4] Chunyang Cheng, Tianyang Xu, Xiao-Jun Wu, Hui Li, Xi Li, Zhangyong Tang, and Josef Kittler. Textfusion: Unveiling the power of textual semantics for controllable image fusion. *Information Fusion*, 117:102790, 2025. 2
- [5] Sung-Jin Cho, Seo-Won Ji, Jun-Pyo Hong, Seung-Won Jung, and Sung-Jea Ko. Rethinking coarse-to-fine approach in single image deblurring, 2021. 3
- [6] Guangmang Cui, Huajun Feng, Zhihai Xu, Qi Li, and Yueting Chen. Detail preserved fusion of visible and infrared images using regional saliency extraction and multi-scale image decomposition. *Optics Communications*, 341:199–209, 2015. 6
- [7] Yanglin Deng, Tianyang Xu, Chunyang Cheng, Xiao-Jun Wu, and Josef Kittler. Mmdrfuse: Distilled mini-model with dynamic refresh for multi-modality image fusion. In *Proceedings of the 32nd ACM International Conference on Multimedia*, page 7326–7335. ACM, 2024. 2, 6, 7
- [8] A.M. Eskicioglu and P.S. Fisher. Image quality measures and their performance. *IEEE Transactions on Communications*, 43(12):2959–2965, 1995. 6
- [9] Zhizhong Fu, Xue Wang, Jin Xu, Ning Zhou, and Yufei Zhao. Infrared and visible images fusion based on rpca and nsct. *Infrared Physics & Technology*, 77:114–123, 2016. 1
- [10] Lin Guo, Xiaoqing Luo, Wei Xie, Zhancheng Zhang, Hui Li, Rui Wang, Zhenhua Feng, and Xiaoning Song. Revisiting generative infrared and visible image fusion based on human cognitive laws. In *The Thirty-ninth Annual Conference on Neural Information Processing Systems*, 2025. 6, 7
- [11] Le Han, Kaixuan Chen, Minchen Ye, and Nenggan Zheng. Hi-motion: Hierarchical intention guided conditional motion synthesis. In *Proceedings of the 33rd ACM International Conference on Multimedia*, pages 9628–9637, 2025. 3
- [12] Le Han, Kaixuan Chen, Lei Zhao, Yangbo Jiang, Pengfei Wang, and Nenggan Zheng. Cross-domain animal pose estimation with skeleton anomaly-aware learning. *IEEE Transactions on Circuits and Systems for Video Technology*, 2025. 2
- [13] Zhanbo Huang, Jinyuan Liu, Xin Fan, Risheng Liu, Wei Zhong, and Zhongxuan Luo. Reconet: Recurrent correction network for fast and efficient multi-modality image fusion. In *Computer Vision – ECCV 2022: 17th European Conference, Tel Aviv, Israel, October 23–27, 2022, Proceedings, Part XVIII*, page 539–555. Springer-Verlag, 2022. 3
- [14] Xinyu Jia, Chuang Zhu, Minzhen Li, Wenqi Tang, and Wenli Zhou. Llvip: A visible-infrared paired dataset for low-light vision. In *Proceedings of the IEEE/CVF International Conference on Computer Vision*, pages 3496–3504, 2021. 5
- [15] Miao Kang, Xiaojun Hu, Weilin Huang, Matthew R. Scott, and Mauricio Reyes. Dual-stream pyramid registration network. *Medical Image Analysis*, 78:102379, 2022. 4
- [16] Alexander Kirillov, Eric Mintun, Nikhila Ravi, Hanzi Mao, Chloe Rolland, Laura Gustafson, Tete Xiao, Spencer Whitehead, Alexander C. Berg, Wan-Yen Lo, Piotr Dollár, and Ross B. Girshick. Segment anything. *2023 IEEE/CVF International Conference on Computer Vision*, pages 3992–4003, 2023. 2, 6
- [17] Hui Li and Xiao-Jun Wu. Multi-focus image fusion using dictionary learning and low-rank representation. In *Image and Graphics*, pages 675–686, 2017. 1
- [18] Hui Li and Xiao-Jun Wu. DenseFuse: A Fusion Approach to Infrared and Visible Images. *IEEE Transactions on Image Processing*, 28(5):2614–2623, 2019. 1, 2
- [19] Hui Li and Xiao-Jun Wu. Crossfuse: A novel cross attention mechanism based infrared and visible image fusion approach. *Information Fusion*, 103:102147, 2024.
- [20] Hui Li, Xiao-Jun Wu, and Tariq Durrani. Nestfuse: An infrared and visible image fusion architecture based on nest connection and spatial/channel attention models. *IEEE Transactions on Instrumentation and Measurement*, 69(12):9645–9656, 2020.
- [21] Hui Li, Xiao-Jun Wu, and Josef Kittler. Rfn-nest: An end-to-end residual fusion network for infrared and visible images. *Information Fusion*, 73:72–86, 2021. 1, 2
- [22] Huafeng Li, Junyu Liu, Yafei Zhang, and Yu Liu. A deep learning framework for infrared and visible image fusion without strict registration. *International Journal of Computer Vision*, 132:1625–1644, 2023. 2, 3, 6, 7
- [23] Hui Li, Tianyang Xu, Xiao-Jun Wu, Jiwen Lu, and Josef Kittler. Lrrnet: A novel representation learning guided fusion network for infrared and visible images. *IEEE Transactions*

- on *Pattern Analysis and Machine Intelligence*, 45(9):11040–11052, 2023. 1, 2
- [24] Huafeng Li, Junzhi Zhao, Jinxing Li, Zhengtao Yu, and Guangming Lu. Feature dynamic alignment and refinement for infrared-visible image fusion: Translation robust fusion. *Information Fusion*, 95:26–41, 2023. 2, 3
- [25] Hui Li, Congcong Bian, Zeyang Zhang, Xiaoning Song, Xi Li, and Xiao-Jun Wu. Occo: Lvm-guided infrared and visible image fusion framework based on object-aware and contextual contrastive learning, 2025. 1
- [26] Huafeng Li, Zengyi Yang, Yafei Zhang, Wei Jia, Zhengtao Yu, and Yu Liu. Mulfs-cap: Multimodal fusion-supervised cross-modality alignment perception for unregistered infrared-visible image fusion. *IEEE Transactions on Pattern Analysis and Machine Intelligence*, 47(5):3673–3690, 2025. 3, 6, 7
- [27] Jing Li, Hongtao Huo, Chang Li, Renhua Wang, and Qi Feng. Attentionfgan: Infrared and visible image fusion using attention-based generative adversarial networks. *IEEE Transactions on Multimedia*, 23:1383–1396, 2021. 2
- [28] Shutao Li, Xudong Kang, and Jianwen Hu. Image fusion with guided filtering. *IEEE Transactions on Image Processing*, 22(7):2864–2875, 2013. 1
- [29] Zhe Li, Haiwei Pan, Kejia Zhang, Yuhua Wang, and Fengming Yu. Mambadfuse: A mamba-based dual-phase model for multi-modality image fusion. *arXiv preprint arXiv:2404.08406*, 2024. 3
- [30] Hanxiao Liu, Zihang Dai, David So, and Quoc V Le. Pay attention to mlps. In *Advances in Neural Information Processing Systems*, pages 9204–9215. Curran Associates, Inc., 2021. 4
- [31] Jinyuan Liu, Xin Fan, Zhanbo Huang, Guanyao Wu, Risheng Liu, Wei Zhong, and Zhongxuan Luo. Target-aware dual adversarial learning and a multi-scenario multi-modality benchmark to fuse infrared and visible for object detection. *Proceedings of the IEEE/CVF Conference on Computer Vision and Pattern Recognition*, pages 5802–5811, 2022. 5
- [32] Jinyuan Liu, Xingyuan Li, Zirui Wang, Zhiying Jiang, Wei Zhong, Wei Fan, and Bin Xu. Promptfusion: Harmonized semantic prompt learning for infrared and visible image fusion. *IEEE/CAA Journal of Automatica Sinica*, 12(3):502–515, 2025. 2
- [33] Yu Liu, Shuping Liu, and Zengfu Wang. A general framework for image fusion based on multi-scale transform and sparse representation. *Information Fusion*, 24:147–164, 2015. 1
- [34] Yu Liu, Xun Chen, Juan Cheng, Hu Peng, and Zengfu Wang. Infrared and visible image fusion with convolutional neural networks. *International Journal of Wavelets, Multiresolution and Information Processing*, 16(03):1850018, 2018. 2
- [35] Haolong Ma, Hui Li, Chunyang Cheng, Gaoang Wang, Xiaoning Song, and Xiaojun Wu. S4fusion: Saliency-aware selective state space model for infrared visible image fusion, 2025. 3, 6, 7
- [36] Jiayi Ma, Wei Yu, Pengwei Liang, Chang Li, and Junjun Jiang. FusionGAN: A generative adversarial network for infrared and visible image fusion. *Information Fusion*, 48: 11–26, 2019. 1, 2
- [37] Jiayi Ma, Han Xu, Junjun Jiang, Xiaoguang Mei, and Xiaoping Zhang. DDcGAN: A Dual-Discriminator Conditional Generative Adversarial Network for Multi-Resolution Image Fusion. *IEEE Transactions on Image Processing*, 29:4980–4995, 2020. 2
- [38] Zhiming Meng, Hui Li, Zeyang Zhang, Zhongwei Shen, Yunlong Yu, Xiaoning Song, and Xiaojun Wu. Comofusion: fast and high-quality fusion of infrared and visible image with consistency model. In *Chinese Conference on Pattern Recognition and Computer Vision (PRCV)*, pages 539–553. Springer, 2024. 3
- [39] Dongyu Rao, Tianyang Xu, and Xiao-Jun Wu. Tgfuse: An infrared and visible image fusion approach based on transformer and generative adversarial network. *IEEE Transactions on Image Processing*, pages 1–1, 2023. 2
- [40] Yun-Jiang Rao. In-fibre bragg grating sensors. *Measurement Science and Technology*, 8(4):355, 1997. 6
- [41] John Roberts, Jan A. N. van Aardt, and Fethi B. Ahmed. Assessment of image fusion procedures using entropy, image quality, and multispectral classification. *Journal of Applied Remote Sensing*, 2, 2008. 6
- [42] Linfeng Tang, Jiteng Yuan, and Jiayi Ma. Image fusion in the loop of high-level vision tasks: A semantic-aware real-time infrared and visible image fusion network. *Information Fusion*, 82:28–42, 2022. 5
- [43] Linfeng Tang, Yuxin Deng, Xunpeng Yi, Qinglong Yan, Yixuan Yuan, and Jiayi Ma. Drmf: Degradation-robust multi-modal image fusion via composable diffusion prior. In *Proceedings of the ACM International Conference on Multimedia*, pages 8546–8555, 2024. 3
- [44] Linfeng Tang, Yeda Wang, Zhanchuan Cai, Junjun Jiang, and Jiayi Ma. Controlfusion: A controllable image fusion framework with language-vision degradation prompts. In *The Thirty-ninth Annual Conference on Neural Information Processing Systems*, 2025. 3
- [45] Linfeng Tang, Qinglong Yan, Xinyu Xiang, Leyuan Fang, and Jiayi Ma. C2rf: Bridging multi-modal image registration and fusion via commonality mining and contrastive learning. *International Journal of Computer Vision*, 133(8): 5262–5280, 2025. 6, 7
- [46] Vibashan Vs, Jeya Maria Jose Valanarasu, Poojan Oza, and Vishal M. Patel. Image fusion transformer. In *2022 IEEE International Conference on Image Processing (ICIP)*, pages 3566–3570, 2022. 2
- [47] Di Wang, Jinyuan Liu, Xin Fan, and Risheng Liu. Unsupervised misaligned infrared and visible image fusion via cross-modality image generation and registration. In *Proceedings of the Thirty-First International Joint Conference on Artificial Intelligence, IJCAI-22*, pages 3508–3515. International Joint Conferences on Artificial Intelligence Organization, 2022. Main Track. 1
- [48] Di Wang, Jinyuan Liu, Long Ma, Risheng Liu, and Xin Fan. Improving misaligned multi-modality image fusion with one-stage progressive dense registration. *IEEE Transactions on Circuits and Systems for Video Technology*, 34(11):10944–10958, 2024. 1, 3, 6, 7
- [49] Zhishe Wang, Zhuoqun Zhang, Wuqiang Qi, Fengbao Yang, and Jiawei Xu. Freqgan: Infrared and visible image fusion

- via unified frequency adversarial learning. *IEEE Transactions on Circuits and Systems for Video Technology*, 35(1): 728–740, 2025. 2, 6, 7
- [50] Housheng Xie, Yukuan Zhang, Junhui Qiu, Xiangshuai Zhai, Xuedong Liu, Yang Yang, Shan Zhao, Yongfang Luo, and Jianbo Zhong. Semantics lead all: Towards unified image registration and fusion from a semantic perspective. *Information Fusion*, page 101835, 2023. 3, 6, 7
- [51] Han Xu, Jiayi Ma, Jiteng Yuan, Zhuliang Le, and Wei Liu. Rfnet: Unsupervised network for mutually reinforcing multi-modal image registration and fusion. In *Proceedings of the IEEE/CVF Conference on Computer Vision and Pattern Recognition*, pages 19679–19688, 2022. 2, 3
- [52] Han Xu, Jiteng Yuan, and Jiayi Ma. Murf: Mutually reinforcing multi-modal image registration and fusion. *IEEE Transactions on Pattern Analysis and Machine Intelligence*, 45(10):12148–12166, 2023. 2, 3, 6, 7
- [53] Jun Yue, Leyuan Fang, Shaobo Xia, Yue Deng, and Jiayi Ma. Dif-fusion: Towards high color fidelity in infrared and visible image fusion with diffusion models, 2023. 3
- [54] Zixiang Zhao, Haowen Bai, Jianshe Zhang, Yulun Zhang, Shuang Xu, Zudi Lin, Radu Timofte, and Luc Van Gool. Cddfuse: Correlation-driven dual-branch feature decomposition for multi-modality image fusion. In *Proceedings of the IEEE/CVF Conference on Computer Vision and Pattern Recognition*, pages 5906–5916, 2023. 2
- [55] Zixiang Zhao, Haowen Bai, Yuanzhi Zhu, Jianshe Zhang, Shuang Xu, Yulun Zhang, Kai Zhang, Deyu Meng, Radu Timofte, and Luc Van Gool. Ddfm: Denoising diffusion model for multi-modality image fusion. In *Proceedings of the IEEE/CVF International Conference on Computer Vision*, pages 8082–8093, 2023. 3
- [56] Xizhou Zhu, Han Hu, Stephen Lin, and Jifeng Dai. Deformable convnets v2: More deformable, better results, 2018. 8
- [57] Xizhou Zhu, Weijie Su, Lewei Lu, Bin Li, Xiaogang Wang, and Jifeng Dai. Deformable detr: Deformable transformers for end-to-end object detection, 2021. 8